PHYSICAL REVIEW B **94**, 174109 (2016)

$Xe(N_2)_2$ compound to 150 GPa: Reluctance to the formation of a xenon nitride

D. Laniel,[*] G. Weck, and P. Loubeyre
CEA, DAM, DIF, F-91297 Arpajon, France

(Received 13 May 2016; revised manuscript received 27 September 2016; published 16 November 2016)

The Xe-N_2 binary phase diagram was determined at 296 K from the pressure evolution of 14 different concentrations. The properties of Xe-N_2 mixtures were characterized using visual observation, Raman spectroscopy, and powder x-ray diffraction. Above 4.9 GPa, the $Xe(N_2)_2$ van der Waals compound is stable and adopts the $MgCu_2$-type Laves phase structure ($Fd\text{-}3m$) with N_2 molecules orientationally disordered. At 10 GPa, this cubic lattice undergoes a martensitic phase transition into a tetragonal ($I4_1/amd$) unit cell. This transition is associated with a partial ordering of the N_2 molecules, possibly due to the growing N_2-N_2 quadrupole-quadrupole interaction with density. No other phase transition was detected up to 154 GPa, even after heating the sample to 2000 K. Above 30 GPa, a softening of the N_2 vibron mode with pressure reveals a weakening of the N_2 intramolecular bond that suggests an electronic redistribution between N_2-N_2 and Xe-N_2 entities. These interactions could explain the great stability of the $Xe(N_2)_2$ compound. However, no xenon nitride was observed.

DOI: 10.1103/PhysRevB.94.174109

I. INTRODUCTION

Pressure is a strong driving force for auto-organization in simple molecular systems. In particular, a new class of molecular solids, i.e., van der Waals compounds, are ubiquitously discovered in molecular mixtures under pressure, whereas they are absent in cryocrystals. Most of the time, their stability can be understood in terms of efficient packing and configuration entropy, similarly to intermetallics or hard-sphere binary compounds [1,2]. N_2 has already been observed to form van der Waals compounds with He [3], Ne [4], and H_2 [5]. However, in nitrogen-based molecular mixtures, efficient packing and configuration entropy considerations solely cannot explain the stability of van der Waals compounds such as $(N_2)_6(Ne)_7$, which has a clathrate-like arrangement of nitrogen molecules [4]. The presence of a strong quadrupole-quadrupole (QQ) interaction between N_2 molecules has to be accounted for.

The noble-gas chemistry of Xe has attracted of lot of interest. At ambient pressure and by relying on specific precursors, xenon can form Xe fluorides [6–8], Xe oxides [9–11], and even Xe nitrides [9,12,13], although the latter have poor thermal stability. Under high pressure, the reactivity of xenon should be greatly enhanced and novel ionic as well as covalent compounds are expected to be formed with many elements [14]. Indeed, XeF_2 [15], Xe hydrides [16], Xe hydrates [17], and Xe oxides [18] have already been observed. The direct interaction of Xe and nitrogen under pressure is predicted to result in a Xe nitride with the XeN_6 stoichiometry [19]. Structurally, XeN_6 is formed by N_6 hexagons and a 12-fold coordination of Xe bonded with nitrogen. Aside from this unusual chemical organization, this Xe nitride should also be a high energy density material. The observation of compounds formation in Xe-N_2 mixtures under pressure is thus promising and of great interest.

In this paper, we demonstrate the existence of a high-pressure van der Waals compound with the $Xe(N_2)_2$ stoichiometry. The binary phase diagram presented here has been determined from the study of 18 Xe-N_2 mixtures with a total of 14 different concentrations. Samples were characterized by synchrotron x-ray diffraction, Raman spectroscopy and visual observation. The remarkable stability of the $Xe(N_2)_2$ compound up to a maximum pressure and temperature of 154 GPa and 2000 K, respectively, could prevent the observation of xenon nitrides predicted under such extreme thermodynamical conditions.

II. Xe-N_2 BINARY PHASE DIAGRAM

Unlike many other rare gas–simple molecule mixtures, Xe-N_2 has not been investigated at low temperatures [20]. At high pressure, the Xe-N_2 phase diagram has been sketched at 408 K from Raman spectroscopy measurements at two concentrations, interestingly suggesting the formation of a stoichiometric compound [21]. Here, we present a detailed determination of the Xe-N_2 binary phase diagram at 296 K. The existence of a stoichiometric compound, $Xe(N_2)_2$, is demonstrated. The experimental procedure is similar to the one used in our previous high-pressure measurements of molecular mixtures [4,22,23]. Membrane diamond anvil cells (DACs), enabling a fine control of pressure to probe structural changes, were equipped with flat anvil culets (500 μm in diameter) and an inox-301 gasket. The cells were then loaded at room temperature in a high-pressure vessel, typically under a pressure of 15 MPa and after sufficient homogenization time (∼12 h). The mixture concentration was estimated from the gases' partial pressures, corrected with the first-order virial coefficients. A ruby microsphere served as a pressure gauge, using the recent quasihydrostatic scale [24]. The uncertainties in pressure and concentration are ±0.05 GPa and ±1 mol %, respectively.

The liquidus phase boundary was determined by visual observation through a microscope apparatus combining pressure measurements. Solid-fluid and fluid-fluid equilibria could easily be observed. The transition points were most finely detected when a single crystal was in equilibrium with the fluid or when a single fluid ball was in equilibrium with another

---

[*] dominique.laniel@cea.fr

fluid. The liquidus line was then delimited by the locus of pressure versus concentration, where the small single crystal or fluid ball was seen to disappear into a homogeneous fluid. As shown in Fig. 1(a), the Xe-N_2 binary phase diagram is of eutectic type with a fluid-fluid phase separation domain. It has two triple points: one corresponding to the equilibrium $F_1 + F_2 + S_{\mathrm{Xe}}$, at 0.7 GPa and 76 mol % Xe, and the other resulting from the equilibrium of $F_1 + S_{\mathrm{Xe}} + \beta$-$N_2$ at 2.6 GPa and 7 mol % Xe.

The nature of the equilibrium in the solid phase was inferred from the combination of visual observation, Raman spectroscopy and powder x-ray diffraction. The latter was performed at the ID09 ($\lambda = 0.4117$ Å) and ID27 ($\lambda = 0.3738$ Å) beamlines of the European Synchrotron Radiation Facility (ESRF). From these measurements, the Xe-rich solid (S_{Xe}) is determined to have the fcc structure of pure solid Xe and to contain a significant amount of N_2. Homogeneous solidification of Xe-rich fluid mixtures containing up to 4 mol % N_2 is observed. Furthermore, the N_2 miscibility in the S_{Xe} alloy increases with pressure. From the volume difference between S_{Xe} (formed from the phase separation in a 6.6 mol % Xe mixture, hence at 2.6 GPa) and pure Xe, it is determined that a maximum of 9.7 mol % N_2 can be inserted into the S_{Xe} solid. A change of N_2 solubility from 4 mol % to 9.7 mol % also produces a difference in the N_2 vibron frequency, as seen in Fig. 1(e). On the other hand, no indication of Xe solubility in the N_2 solid is detected; its N_2 vibron modes, phase transitions, and structures all match those measured in pure solid N_2. Above 4.9 GPa, the formation of a stoichiometric compound is detected from both x-ray diffraction and Raman spectroscopy measurements, as seen in Fig. 1(e) with the emergence of a new Raman mode. From the phase separation equilibria at various concentrations and from the volume of the unit cell, as discussed in the next section, its stoichiometry is inferred to be $\mathrm{Xe(N_2)_2}$. Even after heating a 30 mol % Xe mixture at 200 °C for over a week, $\mathrm{Xe(N_2)_2}$ is still found to coexist with two other solid phases (S_{Xe} and pure N_2). A full recrystallization into the stoichiometric compound seems heavily hindered in the solid state by the diffusion barrier of Xe.

The space filling of hard spheres is used as a guidepost to explain the phase diagram and the formation of compounds in mixtures of molecular systems under pressure [3,23,25]. At 296 K and up to 7 GPa, O_2 and N_2 are highly miscible and form alloys at all concentrations [25]. That is explained by the pronounced orientational disorder of the two molecules in this pressure domain and by their very similar effective pair interactions, inferred from their equations of state [26]. It is thus interesting to compare their binary phase diagram when mixed with Xe. For both mixtures, an AB_2 stoichiometric compound exists, namely $\mathrm{Xe(N_2)_2}$ and $\mathrm{Xe(O_2)_2}$, and have a Laves phase structure. Their stability can be explained by the relationship between their diameter ratio and by the formation of compounds in hard-sphere mixtures [22]. However, their liquidus line is quite different and a fluid-fluid phase separation is only observed for Xe-N_2 mixtures. On the other hand, the $\mathrm{Xe(O_2)_2}$ compound is stable above 3.1 GPa and is apparent on the liquidus line by a peritectic point. In both cases, the solubility of N_2 or O_2 in solid Xe is of a few mol % and increases with pressure, whereas the solubility of Xe in solid N_2 or solid O_2 is less than 1 mol %, if any.

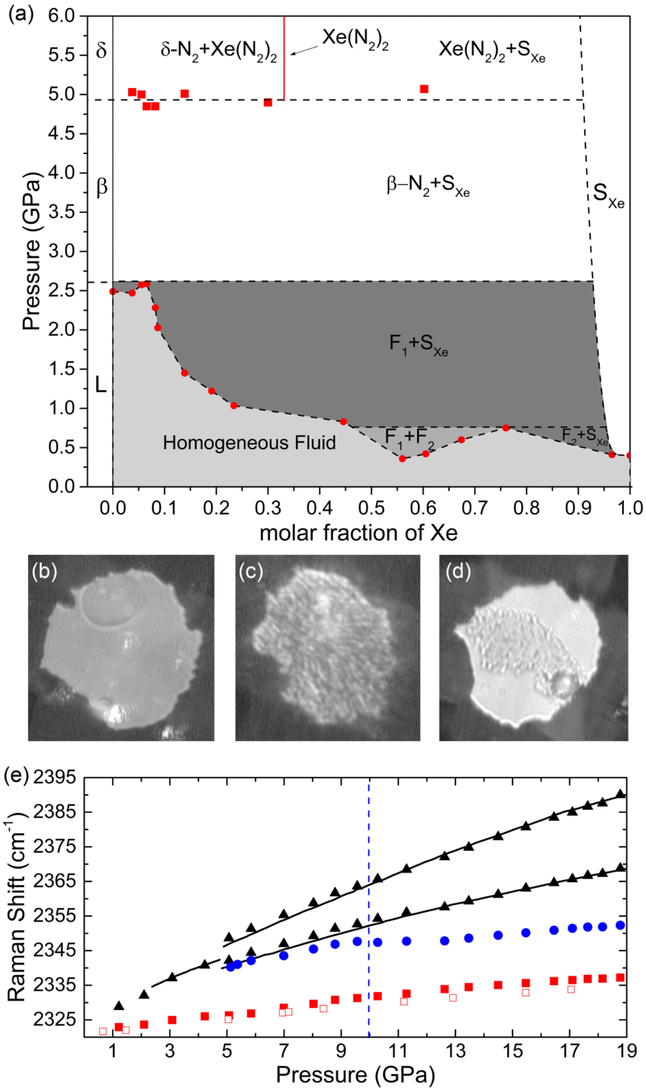

FIG. 1. (a) Binary phase diagram of Xe-N_2. Red dots and squares represent experimental data of the liquidus and of the appearance of the $\mathrm{Xe(N_2)_2}$ solid (error bars in concentration and pressure are smaller than the dots' diameter). The phases of pure nitrogen are indicated on the left-hand side of the diagram. F_1 and F_2 are nitrogen-rich and xenon-rich fluids, respectively, while S_{Xe} is a xenon-rich solid. The $\mathrm{Xe(N_2)_2}$ van der Waals compound is formed at the same pressure (4.9 GPa) as the $\beta \rightarrow \delta$ phase transition in pure nitrogen. (b) Microphotograph of a 67.4 mol % Xe mixture at 0.7 GPa. An F_1 bubble (top) is seen in the F_2 fluid. (c) Microphotograph of a 6.5 mol % Xe mixture at 3.1 GPa. The fine β-N_2 and S_{Xe} powder result from the brutal phase separation occurring at 2.6 GPa. (d) Microphotograph of a 13.9 mol % Xe mixture at 2.1 GPa. The S_{Xe} solid is observed in the F_1 fluid. (e) Raman frequency shift of N_2 vibron modes in different solids with respect to pressure. The black lines represent the vibrational modes of pure N_2 taken from Scheerboom *et al.* [27]. The black triangles, blue dots, and red squares were obtained from pure N_2, $\mathrm{Xe(N_2)_2}$, and S_{Xe}, respectively. The filled symbols were all taken from Xe-N_2 mixtures of 30 mol % Xe. The empty red squares are from a 96 mol % Xe mixture. The Raman shift difference between the empty and filled red squares illustrates the increasing miscibility of N_2 in the xenon-rich solid with pressure. The dashed blue line indicates the phase transition in $\mathrm{Xe(N_2)_2}$, which is noticeable by a weak discontinuity in its N_2 vibron frequency.

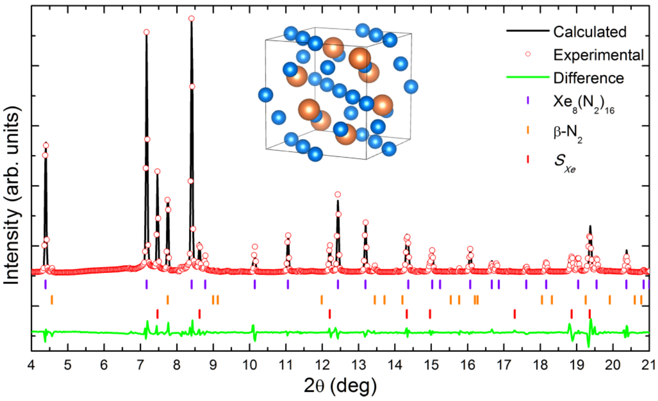

FIG. 2. Powder XRD pattern (λ = 0.4117 Å) obtained from a 6.6 mol % Xe mixture at 4.2 GPa (decompressed from 5.2 GPa) superimposed with its Le Bail refinement. Even at this concentration, three solid phases (S_{Xe}, β-N_2 and $Xe(N_2)_2$) are observed. A cubic (Fd-$3m$) unit cell with a = 9.31 Å fits well the diffraction lines of $Xe(N_2)_2$. The distance between the center of mass of the first-neighbor N_2-N_2 molecules is 3.29 Å, whereas the shortest Xe-N_2 distance is 3.86 Å. (Inset) Drawing of the Laves phase $Xe(N_2)_2$ where the Xe atoms (orange spheres) and the spherically disordered N_2 molecules (blue spheres) occupy the Mg (8a) and Cu (16d) sites, respectively.

III. THE $Xe(N_2)_2$ VAN DER WAALS COMPOUND

A. Cubic phase

The $Xe(N_2)_2$ van der Waals compound was characterized from both powder x-ray diffraction and Raman spectroscopy in the solid-solid phase separation observed above 4.9 GPa for various initial concentrations. Integration of the powder x-ray diffraction images was achieved with the FIT2D [28] and DIOPTAS [29] utilities, while the DICVOL [30], CHEKCELL [31], and XRDA [32] programs were used for their analysis. A Le Bail refinement was performed on a powder x-ray diffraction pattern obtained at 4.2 GPa and is shown in Fig. 2. $Xe(N_2)_2$ was found to have a cubic lattice (Fd-$3m$) with a unit cell volume of V = 806.95 Å^3. That volume is slightly less (0.5%) than the ideal mixing volume ($8 \times V_{Xe} + 16 \times V_{N_2}$) at the same pressure [33,34], which suggests the $Xe(N_2)_2$ stoichiometry. From considerations of maximization of the packing fraction and configurational entropy in hard-sphere mixtures, the AB_2 Laves phase is predicted stable when the hard-sphere radii ratio α is between 0.76 and 0.84, with 0.816 giving the most efficient packing [35]. Nonetheless, Laves phase compounds were experimentally observed in solids for a broader range of α values (from 0.6 to 0.95) [36]. Although first detected in metallic binary phases, Laves phases are also a common occurrence in van der Waals molecular compounds such as $Xe(O_2)_2$ [22], $CH_4(H_2)_2$ [37], and $Ar(H_2)_2$ [38], under pressure. Indeed, in the $CH_4(H_2)_2$ and $Ar(H_2)_2$ compounds, the molecular constituents are orientationally disordered and so are roughly approximated by hard spheres. At 5.5 GPa, the xenon-nitrogen van der Waals compound has a $\alpha = 0.88$, which nears the predicted range of values for which hard-sphere-like compounds are stable. Among the three possible Laves phases, only the one isomorphous to the $MgCu_2$ structure has a cubic Fd-$3m$ unit cell. Thus, we propose that $Xe_8(N_2)_{16}$ adopts the $MgCu_2$-type Laves phase structure, with the Xe and N_2 entities occupying the Mg (8a) and Cu (16d) sites, respectively. The same structure was attributed to $Xe(O_2)_2$ [22].

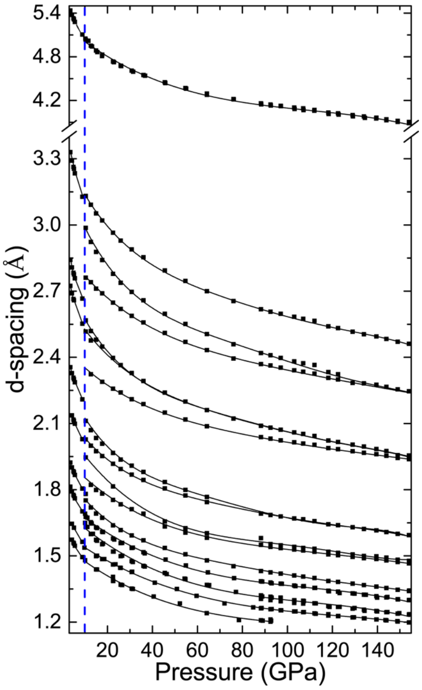

FIG. 3. Evolution of the $Xe(N_2)_2$ compound d-spacings with pressure. The dotted blue line at 10 GPa evidences the d-spacing discontinuities associated with a cubic-to-tetragonal martensitic phase transition.

$Xe(N_2)_2$ adopts a structure that is understood by representing its constituents as hard spheres. The N_2 molecules are thus thought to be spherically disordered (as drawn in Fig. 2), which is consistent with the low-pressure phases of pure N_2 [39,40]. Attempts to confirm these atomic positions from a Rietveld refinement were unsuccessful, mainly due to preferential orientations of $Xe(N_2)_2$ crystallites.

B. Tetragonal phase

At 10 GPa, $Xe(N_2)_2$ undergoes a phase transition characterized by discontinuities in the d-spacings (Fig. 3) and a weak anomaly on the pressure evolution of the Raman frequency shift [Fig. 1(e)]. The high-pressure phase was found to have the tetragonal $I4_1/amd$ space group with lattice parameters a = 5.982(1) Å and c = 9.338(1) Å [V = 334.15(3) Å^3] at 10.3 GPa. The volume of this new lattice is less (2.1%) than the ideal volume of mixing ($4 \times V_{Xe} + 8 \times V_{N_2}$) at the same pressure, which suggests the same $Xe(N_2)_2$ stoichiometry as the low-pressure phase. The tetragonal structure is obtained by a distortion of the low-pressure cubic lattice: a compression along the a and b axes, compensated by an elongation along the c axis. The martensitic phase transition explains why many of the d-spacings are continuous through the phase transition while only a few new diffraction lines appear, and why the N_2 vibron frequency is only slightly perturbed. The same transformation was previously identified in another $MgCu_2$-type Laves phase, $CaLi_2$ [41]. Furthermore, identifying the distortion process advocates for Xe atoms and N_2 molecules

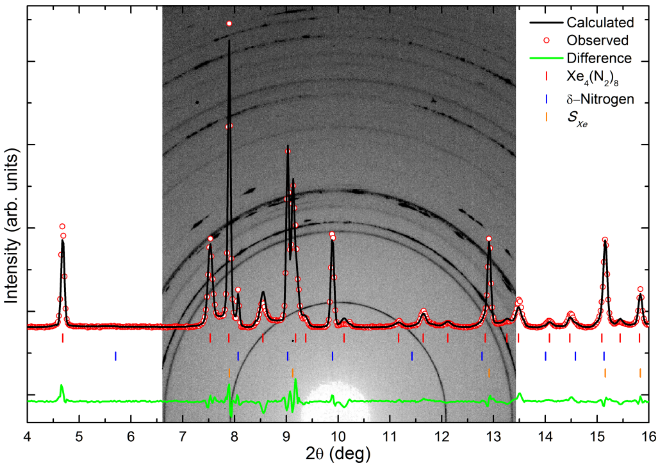

FIG. 4. Rietveld refinement of tetragonal ($I4_1/amd$) $Xe(N_2)_2$ at 10.3 GPa. The image plate corresponding to the refined diffraction pattern is in the background. The diffraction pattern was obtained from a 6.6 mol % Xe mixture with a wavelength of $\lambda = 0.4117$ Å. The $Xe(N_2)_2$ powder is of great quality, whereas the diffraction rings of solid N_2 and S_{Xe} show a nonhomogeneous crystallite distribution. The reliability factors for the refinement are $R_{wp} = 17.2\%$ and $R_{\mathrm{exp}} = 18.1\%$, which yields a satisfactory goodness of fit of 0.95.

center of mass to be on the 4*b* and 8*c* Wyckoff sites, respectively, based on the suggested cubic structure.

A Rietveld refinement of a powder x-ray diffraction pattern obtained at 10.3 GPa (see Fig. 4) was performed using FULLPROF [42]. Although many different positions for the Xe atoms and N_2 molecules center of mass were tested out, those suggested from the martensitic transformation yielded the best results. From there, the rigid body function was used to allow nitrogen molecules to freely explore all orientations about their center of mass. Their state of disorder was determined by adding additional molecules on the same center of mass (and correcting with the appropriate fractional occupancy) to see if it improved the quality of the fit. A partial orientational order gave a better adjustment than the one for isotropically distributed molecules. The intramolecular N_2 bond length was fixed to 1.09 Å, which is a typical value at this pressure [40]. Atomic positions determined from the Rietveld refinement are listed in Table I, and the corresponding crystal structure is drawn in Fig. 5.

While hard-sphere packing considerations mainly explain the stability of $Xe(N_2)_2$ below 10 GPa, the QQ interaction between N_2 molecules also needs to be taken into account. Mostly relevant in the density domain where van der Waals interactions dominate, it increases along with pressures. The QQ interaction tends to reduce the disorder and orient the N_2 molecular axes, as found in pure nitrogen [40,45] as well as in most N_2-based van der Waals compounds [4,40,46]. As seen in Fig. 5, N_2 molecules in $Xe(N_2)_2$ also align themselves in the tetragonal phase.

In the $Xe(N_2)_2$ cubic compound, the spherically disordered nitrogen molecules form four sets of interpenetrating layers of kagome nets. The tetragonal distortion deforms the kagome nets, resulting in N_2 hexagons having two N_2-N_2 distances that are slightly shorter (7%) than the four others [see Fig. 5(b)]. For this specific geometry, we here observe that the QQ interaction favors the slipped-parallel energy-minimizing configuration [47]. Also, the nitrogen molecules are slightly tilted in order to maximize their distance with xenon atoms. Thus, it is clear that QQ interaction plays an important role in the cubic-to-tetragonal phase transition, since (i) it occurs at pressures where van der Waals interactions still dominate, (ii) the molecular disorder is greatly reduced after the phase transition, and (iii) the orientation of the N_2 molecules in the tetragonal phase minimizes the QQ interaction. While quadrupolar orders in a hexagonal plane have been fully studied [48], no theoretical predictions of quadrupolar orders in a kagome lattice have been published, which contrasts with an extensive literature for dipolar orders [49]. The N_2 order observed here could be an experimental solution for this problem that should now motivate further theoretical studies.

C. High-pressure evolution

The pressure evolution of the tetragonal cell of $Xe(N_2)_2$ was followed by x-ray diffraction and Raman spectroscopy up to 154 GPa and 141 GPa, respectively. For these experiments, bevel diamond anvils with a 70 μm culet were used. The diamond anvil cells were loaded in a high-pressure vessel at about 150 MPa after an adequate homogenization time of the mixture. Gold and ruby microspheres placed in the sample chamber were used as pressure gauges [24,50].

Up to the highest measured pressure, no phase transition was observed in the tetragonal lattice. Twelve diffraction lines of $Xe(N_2)_2$ were tracked up to 154 GPa and used to calculate the unit cell volume, shown as a function of pressure in Fig. 6. The data points were fitted by a Vinet equation of state with the following parameters: $B_0 = 4.9(1)$ GPa, $B_0' = 6.0(1)$, and $V_0 = 562.04(2)$ Å^3. The bulk modulus and its derivative are close to the values of pure fcc and hcp xenon, which are $B_0 = 4.887$ GPa, $B_0' = 6.1805$, and $B_0 = 4.887$ GPa, $B_0' = 6.2955$, respectively [43]. The measured volume of $Xe(N_2)_2$ is compared to the ideal mixing volume and is found smaller. Overall, the volume difference grows as a function of pressure, hinting that $Xe(N_2)_2$ is increasingly energetically favored compared to the pure compounds.

TABLE I. Structural parameters of $Xe(N_2)_2$ at 10.3 GPa and 296 K. Space group $I4_1/amd$, $a = b = 5.982(1)$ Å and $c = 9.338(1)$ Å ($V = 334.15(3)$ Å^3).

Atoms	Wyckoff site	*x*	*y*	*z*	Site occupancy	B_{iso}
Xe	4*b*	0	0.25	0.375	1	1.55(3)
N1	32*i*	0.238(2)	0.252(2)	0.809(2)	1/4	0.51(3)
N2	32*i*	0.272(2)	0.229(2)	0.687(2)	1/4	0.51(3)

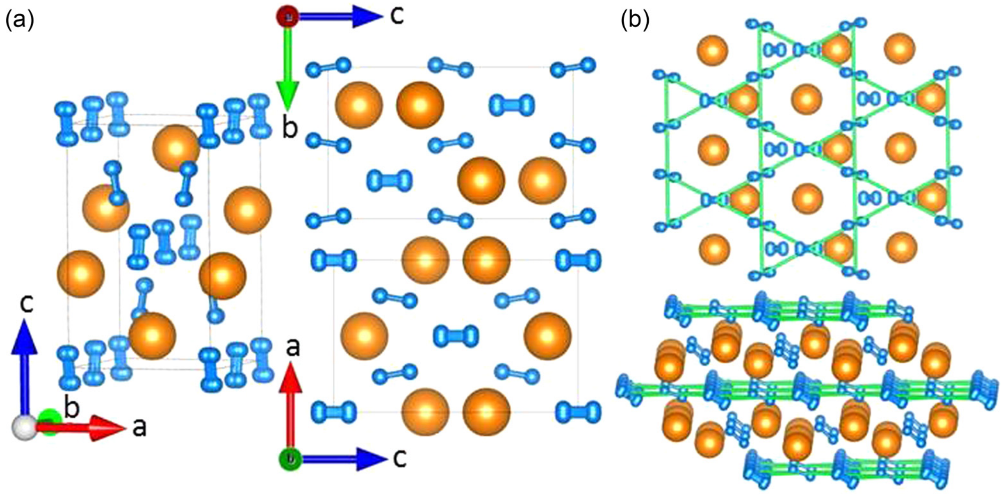

FIG. 5. Tetragonal ($I4_1/amd$) structure of Xe(N$_2$)$_2$ at 10.3 GPa. Xenon and nitrogen atoms are drawn as orange and blue spheres, respectively. (a) The nitrogen molecules are found only partially disordered after the phase transition. The disorder of the nitrogen molecules is modeled by an overlap of each of the nitrogen molecules with three others: one N$_2$ center of mass is occupied by a total of four molecules. When taking into account the occupancy of a nitrogen atom (0.25), each N$_2$ center of mass is effectively occupied by a single molecule, with a slightly varying orientation, representing the N$_2$ molecule partial disorder. Each Xe atom has four Xe nearest neighbors at distances larger (3.51 Å) than in pure Xe at the same pressure (3.38 Å) [43]. The shortest Xe-N$_2$ and N$_2$-N$_2$ distances (position of the center of mass was used for the N$_2$ molecules) are of 3.55 Å and 2.99 Å, respectively. (b) Distorted kagome nets in the tetragonal Xe(N$_2$)$_2$ structure. (Top) Top view of a distorted kagome plane. N$_2$ hexagons and N$_2$ triangles forming the distorted kagome lattice have two and one slightly shorter N$_2$-N$_2$ distances (7%), respectively. (Bottom) Side view of the kagome planes, which emphasizes the layered arrangement of kagome layer's nets of N$_2$ molecules and puckered sheets of Xe. N$_2$ molecules are interpreted to align due to the QQ interaction, known to minimize the energy with the slipped-parallel configuration. The orientation of the molecules was validated with a Rietveld refinement at both 10.3 and 30.0 GPa. Drawings were done using the VESTA software [44].

Raman spectroscopy measurements performed in a 30 mol % Xe mixture to 141 GPa are shown in Figs. 7 and 8. Although Xe(N$_2$)$_2$ is the dominant compound in the sample chamber, spectra obtained from different regions revealed vibrons corresponding to pure solid N$_2$ and S_{Xe}. Above 20 GPa and well into the megabar regime, three N$_2$ vibrational modes of Xe(N$_2$)$_2$ are clearly observed. The lowest frequency mode is intense, while the two others are weak. With a laser excitation wavelength of 488 nm, sample luminescence is detected from ~40 GPa and amplifies concomitantly with an increase in opacity. By ~60 GPa, the luminescence becomes more important than the Raman signal of the diamond anvils. Between 60.2 and 81.6 GPa, a near-infrared laser excitation wavelength (1064 nm) had to be used and only the strongest Xe(N$_2$)$_2$ vibration mode could be followed. Above 85 GPa, due to the redshift of the luminescence band with pressure, Raman spectra could again be obtained with the 488 nm laser excitation wavelength. As pressure is further increased, the Raman signal progressively diminishes in intensity and the peaks widen to the point where the strongest vibrational mode can barely be distinguished at 141 GPa. At this pressure, the sample is completely opaque (see inset of Fig. 8). This change in opacity has to be attributed to Xe(N$_2$)$_2$, since a 11 mol % Xe mixture, constituted only of Xe(N$_2$)$_2$ and pure N$_2$ at higher pressures, also becomes dark at similar pressures, while pure N$_2$ is still transparent at 140 GPa [54]. Decompression of the Xe(N$_2$)$_2$ compound, laser-heated to 2000 K, displayed a complete reversibility of the sample's opacity as well as of the intensity and frequency of its principal Raman modes (see Fig. 7).

Remarkably, the lowest frequency vibron of Xe(N$_2$)$_2$ suffers significant softening with compression. Starting from ~30 GPa, it drops below gaseous N$_2$ vibrational frequency at ~80 GPa and goes down to 2207 cm^{-1} at 141 GPa. The two other N$_2$ vibrational modes of Xe(N$_2$)$_2$ follow a trend much more similar to the lowest frequency vibron of pure N$_2$.

D. Towards a xenon nitride

The vibron mode softening of a molecule under pressure typically indicates a weakening of the intramolecular bonding between its constituents. Observed in Xe-O$_2$ [43] and pure N$_2$ [54] systems under pressure, this softening has been ascribed to an electronic density redistribution between the molecular bond and its neighboring atoms. This electronic modification also induces an increased absorption of the visible light. In Xe(N$_2$)$_2$, the complete darkening and the N$_2$ bond weakening are interpreted as similar signs of a perturbation of the N$_2$ intramolecular electronic density due to a growing interaction between N$_2$-N$_2$ and Xe-N$_2$ entities. The N$_2$-N$_2$ interaction in Xe(N$_2$)$_2$ is gauged from observations in pure solid nitrogen under pressure. The lowest vibron frequency in pure nitrogen begins to redshift at ~80 GPa [54], corresponding to intermolecular distances of about 1.93 Å [56]. In Xe(N$_2$)$_2$, a very similar N$_2$-N$_2$ intermolecular distance (1.97 Å) is observed at only 30.0 GPa, pressure at which the N$_2$ vibron frequency redshifts and hence the N$_2$ bond weakening is first detected. Thus, we interpret the start of the vibron frequency redshift in Xe(N$_2$)$_2$ as a pressure-induced electronic redistribution between neighboring N$_2$ molecules.

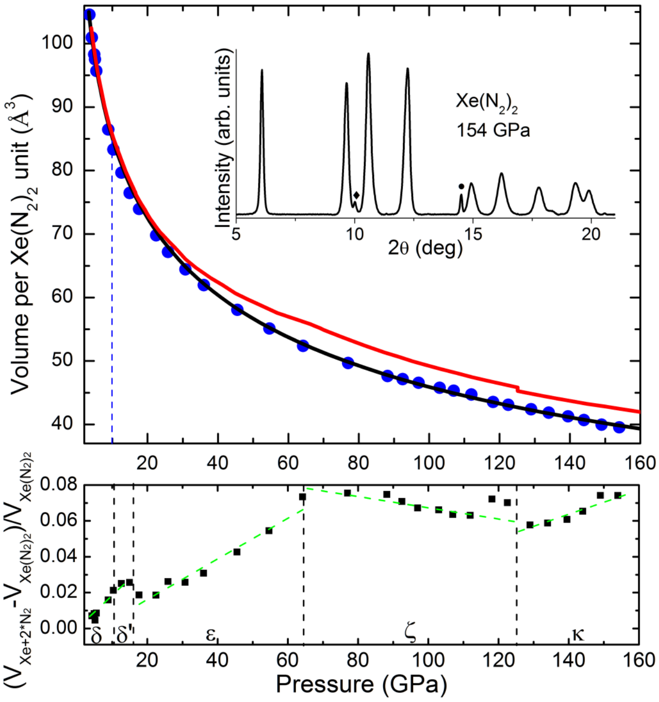

FIG. 6. (Top) Volume of $Xe(N_2)_2$ with respect to pressure. Measurements were made in a 30 mol % Xe mixture. The black line is a Vinet equation of state fit of the data points (blue dots) corresponding to the tetragonal $Xe(N_2)_2$ solid. The red line is the ideal volume of mixing, $V_{Xe} + 2V_{N_2}$, obtained from the equations of states of the pure systems [51–53]. The discontinuity around 125 GPa corresponds to the $\zeta \rightarrow \kappa$ phase transition in pure nitrogen. Literature data were updated with the latest ruby pressure scale [24]. (Inset) Diffraction pattern obtained on a 30 mol % Xe mixture at 154 GPa with a wavelength of $\lambda = 0.3738$ Å. The black lozenge and circle represent diffraction lines from the xenon-rich solid and LiF, respectively. LiF was used as a thermal insulator. (Bottom) Volume difference between the $Xe(N_2)_2$ structure and the ideal volume of mixing, $V_{Xe} + 2V_{N_2}$. The phases of pure nitrogen are indicated and its phase transitions marked by vertical dashed lines.

This interaction is not thought to be dominant at pressures lower than 30 GPa.

In pure N_2, this intermolecular interaction leads to the formation of single-bonded N polymeric phases (cg-N and LP-N) [57,58]. These polymeric phases are obtained at pressures and temperatures above 110 GPa and 2000 K. The $Xe(N_2)_2$ compound was laser-heated to 2000 K at 154 GPa using thin LiF layers on the anvils' culet to thermally insulate the sample from the diamonds. Puzzlingly, no formation of a single-bonded form of nitrogen was observed. Instead, a more complete transformation of the 30 mol % Xe solid into the $Xe(N_2)_2$ compound was detected. Hence, $Xe(N_2)_2$ is the stable phase under such thermodynamic conditions. Moreover, it implies that in this pressure range, electronic contributions other than van der Waals interactions between Xe and N_2 must be taking part in stabilizing the structure.

The Xe-N_2 interaction is gauged by looking at S_{Xe} in which the weakening of the intramolecular N_2 bond is also noticed by a redshift observed above 30 GPa (see Fig. 7). Since the fraction of N_2 molecules is low in S_{Xe} [see

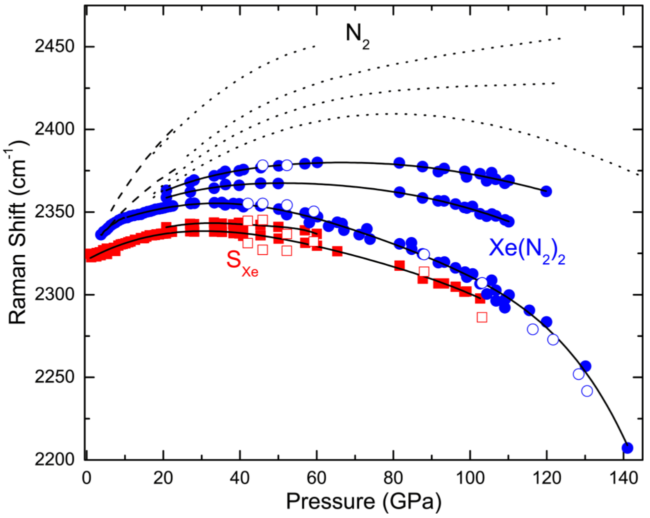

FIG. 7. Raman shift of N_2 vibron modes in different solids with respect to pressure. Data were obtained from mixtures with concentrations between 11 and 30 mol % Xe. The red squares and blue circles were obtained from S_{Xe} and $Xe(N_2)_2$, respectively. The filled symbols represent data points taken during compression, while the empty ones were acquired during sample decompression. The black dashed and dotted lines are the pure N_2 vibrational modes taken from Schneider *et al.* [55] and Goncharov *et al.* [54], respectively. Around 110 GPa, the Raman mode of the S_{Xe} solid is overlapped by the more intense vibrational mode of $Xe(N_2)_2$. Mixtures of 11 mol % Xe, which showed none of the S_{Xe} Raman modes allowed to confirm that the vibron observed above 110 GPa belongs to $Xe(N_2)_2$.

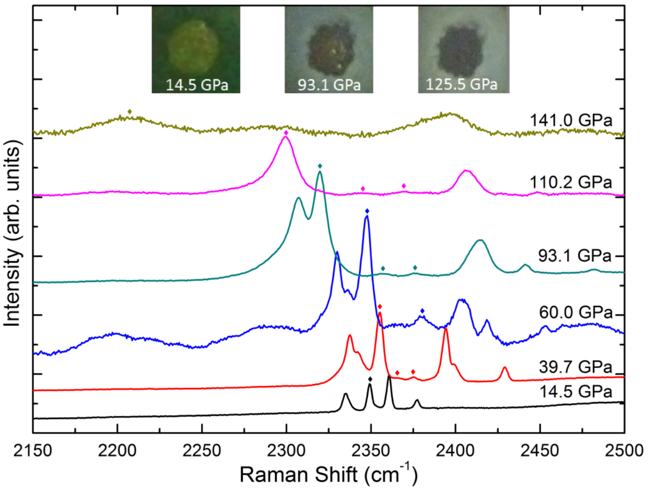

FIG. 8. Raman spectrum of a 30 mol % Xe mixture at selected pressures. An offset on the vertical axis was applied to improve clarity. Lozenges indicate the $Xe(N_2)_2$ vibrational modes. The modes at higher frequency belong to pure solid N_2, while the ones at lower frequency belong to S_{Xe}. The oscillations found in the spectra at 60.0 GPa are caused by the strong fluorescence emanating from the sample. From 100 GPa, the main Raman mode of S_{Xe} is overlapped by the $Xe(N_2)_2$ vibrational mode. At 141 GPa, the $Xe(N_2)_2$ main vibron becomes of lower intensity than the pure N_2 vibrational mode, which is a consequence of the N_2 intramolecular bond weakening. (Inset) Microphotographs of a 30 mol % Xe mixture, illuminated in both transmission and reflection. At 125.5 GPa, the sample becomes completely dark. Light only goes through the ruby ball.

Fig. 1(a)], the interaction between neighboring N_2 is highly unlikely to induce an intramolecular bond weakening. Thus, the weakening is interpreted as due to the Xe-N_2 chemical interaction. When the redshift begins in S_{Xe}, a first-neighbor distance of ~2.82 Å (at 30.0 GPa) is measured between N and Xe atoms. In $Xe(N_2)_2$, the same Xe-N distance is reached at around 65 GPa. Consequently, from this pressure, a Xe-N_2 interaction is also thought to occur in $Xe(N_2)_2$ and increases its stability. This is analogous to the redistribution of electronic density observed in the $Xe(H_2)_8$ compound, which was interpreted to make it stable up to 255 GPa [16].

Recently published numerical simulations of the convex hull of Xe-N_2 compounds predict the synthesis of the XeN_6 xenon nitride from any concentration of Xe-N_2 mixtures when compressed above 146 GPa at ambient temperature or beyond 132 GPa at 2500 K [19]. Under similar pressure-temperature conditions, we here observe the remarkable stability of the $Xe(N_2)_2$ compound. Either the thermodynamical conditions for the formation of XeN_6 were underestimated in the calculations or the $Xe(N_2)_2$ compound is completely modifying the convex hull for the formation of Xe-N compounds. Further theoretical and experimental works are needed to disclose this issue.

IV. CONCLUSION

We have performed a thorough investigation of Xe-N_2 mixtures up to 154 GPa and 2000 K. The binary phase diagram, resolved with 14 different mixture concentrations, is shown to be of eutectic type with two triple points. A Laves phase van der Waals compound with the $Xe(N_2)_2$ stoichiometry is found stable. Its stability is first explained by the efficient packing of a hard-sphere binary mixture. At 10 GPa, cubic $Xe(N_2)_2$ undergoes a martensitic phase transition into a tetragonal structure with a partial ordering of the N_2 molecules that is probably due to the growing influence of the QQ interaction under pressure. As pressure is further increased to 154 GPa, $Xe(N_2)_2$ preserves its crystalline structure, although a redistribution of electronic density occurs between N_2-N_2 and Xe-N_2 entities. This is identified by a significant softening of the N_2 vibrational frequency coupled with a complete sample darkening. The Xe-N_2 interaction could explain the remarkable stability of the $Xe(N_2)_2$ compound under thermodynamical conditions for which the N_2 triple bond should break and the XeN_6 xenon nitride is expected to form. Calculations are now needed to properly map out the electronic density redistribution and identify exactly how $Xe(N_2)_2$ is more stable than a xenon-nitrogen bonded solid in the 150 GPa pressure range.

ACKNOWLEDGMENTS

The authors gratefully acknowledge the Centre National d'Études Spatiales (CNES) for funding the Ph.D. of D.L. The authors also acknowledge the European Synchrotron Radiation Facility (ESRF) for provision of beamtime under proposals HC-1890 as well as HC-2182, and thank G. Garbarino for his technical assistance on the ID09A and ID27 beamlines of the ESRF.

---

[1] W. Hume-Rothery and R. E. Smallman, *The Structure of Metals and Alloys* (The Institute of Metals, London, 1969).
[2] B. J. Alder, W. E. Alley, and M. Rigby, Physica **73**, 143 (1974).
[3] W. L. Vos, L. W. Finger, R. J. Hemley, J. Z. Hu, H. K. Mao, and J. A. Schouten, Nature (London) **358**, 46 (1992).
[4] T. Plisson, G. Weck, and P. Loubeyre, Phys. Rev. Lett. **113**, 025702 (2014).
[5] D. K. Spaulding, G. Weck, P. Loubeyre, F. Datchi, P. Dumas, and M. Hanfland, Nat. Commun. **5**, 5739 (2014).
[6] J. G. Malm, I. Sheft, and C. L. Chernick, J. Am. Chem. Soc. **85**, 110 (1963).
[7] H. H. Claassen, H. Selig, and J. G. Malm, J. Am. Chem. Soc. **84**, 3593 (1962).
[8] M. A. Tius, Tetrahedron **51**, 6605 (1995).
[9] J. M. Whalen and G. J. Schrobilgen, J. Fluor. Chem. **71**, 225 (1995).
[10] M. V. Ivanova, H. P. A. Mercier, and G. J. Schrobilgen, J. Am. Chem. Soc. **137**, 13398 (2015).
[11] G. J. Schrobilgen and J. M. Whalen, Inorg. Chem. **33**, 5207 (1994).
[12] A. A. A. Emara and G. J. Schrobilgen, J. Chem. Soc., Chem. Commun., 257 (1988).
[13] G. L. Smith, H. P. A. Mercier, and G. J. Schrobilgen, Inorg. Chem. **47**, 4173 (2008).
[14] L. Zhu, H. Liu, C. J. Pickard, G. Zou, and Y. Ma, Nat. Chem. **6**, 644 (2014).
[15] M. Kim, M. Debessai, and C.-S. Yoo, Nat. Chem. **2**, 784 (2010).
[16] M. Somayazulu, P. Dera, A. F. Goncharov, S. A. Gramsch, P. Liermann, W. Yang, Z. Liu, H.-K. Mao, and R. J. Hemley, Nat. Chem. **2**, 50 (2010).
[17] C. Sanloup, S. A. Bonev, M. Hochlaf, and H. E. Maynard-Casely, Phys. Rev. Lett. **110**, 265501 (2013).
[18] A. Dewaele, N. Worth, C. J. Pickard, R. J. Needs, S. Pascarelli, O. Mathon, M. Mezouar, and T. Irifune, Nat. Chem **8**, 784 (2016).
[19] F. Peng, Y. Wang, H. Wang, Y. Zhang, and Y. Ma, Phys. Rev. B **92**, 094104 (2015).
[20] A. I. Prokhvatilov, I. Y. Minchina, and L. D. Yantsevich, *Handbook of Binary Solutions of Cryocrystals* (Begell House, New York, 1996).
[21] M. E. Kooi and J. A. Schouten, Phys. Rev. B **60**, 12635 (1999).
[22] G. Weck, A. Dewaele, and P. Loubeyre, Phys. Rev. B **82**, 014112 (2010).
[23] P. Loubeyre, M. Jean-Louis, R. LeToullec, and L. Charon-Gérard, Phys. Rev. Lett. **70**, 178 (1993).
[24] A. Dewaele, M. Torrent, P. Loubeyre, and M. Mezouar, Phys. Rev. B **78**, 104102 (2008).
[25] D. Sihachakr and P. Loubeyre, Phys. Rev. B **70**, 134105 (2004).
[26] F. H. Ree, *Simple Molecular Systems at Very High Density*, edited by A. Polian, P. Loubeyre, and N. Boccara (Plenum Press, New York, 1989).

[27] M. I. M. Scheerboom and J. A. Schouten, J. Chem. Phys. **105**, 2553 (1996).
[28] A. P. Hammersley, S. O. Svensson, M. Hanfland, A. N. Fitch, and D. Hausermann, High Press. Res. **14**, 235 (1996).
[29] C. Prescher and V. B. Prakapenka, High Press. Res. **35**, 223 (2015).
[30] A. Boultif and D. Louër, J. Appl. Crystallogr. **24**, 987 (1991).
[31] J. Laugier and B. Bochu, LMGP Suite of Programs for the Interpretation of X-ray Experiments, http://www.inpg.fr/LMGP.
[32] S. Desgreniers and K. Lagarec, J. Appl. Crystallogr. **27**, 432 (1994).
[33] A. N. Zisman, I. V. Aleksandrov, and S. M. Stishov, Pis'ma Zh. Eksp. Teor. Fiz. **40**, 253 (1984).
[34] R. L. Mills, B. Olinger, and D. T. Cromer, J. Chem. Phys. **84**, 2837 (1986).
[35] A.-P. Hynninen, L. Filion, and M. Dijkstra, J. Chem. Phys. **131**, 64902 (2009).
[36] J. H. Zhu, C. T. Liu, L. M. Pike, and P. K. Liaw, Metall. Mater. Trans. A **30**, 1449 (1999).
[37] M. Somayazulu, L. W. Finger, R. J. Hemley, and H. Mao, Science **271**, 1400 (1996).
[38] P. Loubeyre, R. Letoullec, and J.-P. Pinceaux, Phys. Rev. Lett. **72**, 1360 (1994).
[39] D. Schiferl, D. T. Cromer, R. R. Ryan, A. C. Larson, R. LeSar, and R. L. Mills, Acta Crystallogr. C **39**, 1151 (1983).
[40] G. W. Stinton, I. Loa, L. F. Lundegaard, and M. I. McMahon, J. Chem. Phys. **131**, 104511 (2009).
[41] J. Feng, N. W. Ashcroft, and R. Hoffmann, Phys. Rev. Lett. **98**, 247002 (2007).
[42] H. M. Rietveld, J. Appl. Crystallogr. **2**, 65 (1969).
[43] A. Dewaele, P. Loubeyre, P. Dumas, and M. Mezouar, Phys. Rev. B **86**, 014103 (2012).
[44] K. Momma and F. Izumi, J. Appl. Crystallogr. **44**, 1272 (2011).
[45] A. Mulder, J. P. J. Michels, and J. A. Schouten, J. Chem. Phys. **105**, 3235 (1996).
[46] S. Ninet, G. Weck, P. Loubeyre, and F. Datchi, Phys. Rev. B **83**, 134107 (2011).
[47] R. G. A. Bone and N. C. Handy, Theor. Chim. Acta **78**, 133 (1990).
[48] S. E. Roosevelt and L. W. Bruch, Phys. Rev. B **41**, 12236 (1990).
[49] J. L. Atwood, Nat. Mater. **1**, 91 (2002).
[50] K. Takemura and A. Dewaele, Phys. Rev. B **78**, 104119 (2008).
[51] H. Cynn, C. S. Yoo, B. Baer, V. Iota-Herbei, A. K. McMahan, M. Nicol, and S. Carlson, Phys. Rev. Lett. **86**, 4552 (2001).
[52] H. Olijnyk, J. Chem. Phys. **93**, 8968 (1990).
[53] E. Gregoryanz, A. F. Goncharov, C. Sanloup, M. Somayazulu, H. K. Mao, and R. J. Hemley, J. Chem. Phys. **126**, 184505 (2007).
[54] A. F. Goncharov, E. Gregoryanz, H. K. Mao, Z. Liu, and R. J. Hemley, Phys. Rev. Lett. **85**, 1262 (2000).
[55] H. Schneider, W. Häfner, A. Wokaun, and H. Olijnyk, J. Chem. Phys. **96**, 8046 (1992).
[56] M. I. Eremets, A. G. Gavriliuk, N. R. Serebryanaya, I. A. Trojan, D. A. Dzivenko, R. Boehler, H. K. Mao, and R. J. Hemley, J. Chem. Phys. **121**, 11296 (2004).
[57] M. I. Eremets, A. G. Gavriliuk, I. A. Trojan, D. A. Dzivenko, and R. Boehler, Nat. Mater. **3**, 558 (2004).
[58] D. Tomasino, M. Kim, J. Smith, and C.-S. Yoo, Phys. Rev. Lett. **113**, 205502 (2014).